Applied Catalysis B: Environmental 152–153 (2014) 202–211

Contents lists available at ScienceDirect

Applied Catalysis B: Environmental

journal homepage: www.elsevier.com/locate/apcatb

The effect of calcination temperature on structure and photocatalytic properties of Au/Pd nanoparticles supported on TiO_2

Anna Cybula[a], Jacqueline B. Priebe[b], Marga-Martina Pohl[b], Janusz W. Sobczak[c], Matthias Schneider[b], Anna Zielińska-Jurek[a], Angelika Brückner[b], Adriana Zaleska[a,*]

[a] Department of Chemical Technology, Gdansk University of Technology, 80-233 Gdansk, Poland
[b] Leibniz Institute for Catalysis at the University of Rostock, D-18059 Rostock, Germany
[c] Mazovia Center for Surface Analysis, Institute of Physical Chemistry, Polish Academy of Sciences, 01-224 Warsaw, Poland

ARTICLE INFO

Article history:
Received 13 November 2013
Received in revised form 10 January 2014
Accepted 15 January 2014
Available online 28 January 2014

Keywords:
$Au/Pd–TiO_2$ nanoparticles
Metal re-distribution
In-situ EPR
Photocatalysis

ABSTRACT

TiO_2 modified with Au/Pd nanoparticles have been prepared using a water-in-oil microemulsion system of water/AOT/cyclohexane followed by calcination from 350 to 700 °C. The photocatalysts were characterized by scanning transmission electron microscopy (STEM), X-ray powder diffraction analysis (XRD), UV–vis diffuse-reflectance spectroscopy (DRS), BET surface area measurements and X-ray photoelectron spectroscopy (XPS). In-situ EPR spectroscopy was used to examine the relevance of paramagnetic species formation at the surface of $Au/Pd–TiO_2$ photocatalysts under visible (vis) and UV–vis light excitation. The results show that enhancement of calcination temperature from 350 to 700 °C resulted in a slight drop of $Au/Pd–TiO_2$ photoactivity under UV and quite rapid drop under visible light. The $Au/Pd–TiO_2$ samples calcinated at 350 and 400 °C possess the highest photocatalytic activity when degrading phenol under visible light, which is more than 4 times of that of calcinated at 450 °C. It was observed that increasing temperature from 350 to 700 °C during calcination step, caused to segregation of metals and gold-enrichment in the shell region of Au/Pd bimetallic nanoparticles formed at the TiO_2 surface and finally resulted in photoactivity drop. The Pd to Au ratio in the surface layer of Au/Pd nanoparticles decreased from 5:1 to 1:4 with temperature enhancement from 350 to 700 °C, respectively. Based on EPR spectra, it seems that formation of $O^{\bullet -}$ radicals is mainly responsible for phenol degradation under UV light for all $Au/Pd–TiO_2$ samples, since organic radicals could be related to phenol degradation under visible light.

1. Introduction

Bimetallic nanoparticles, composed of two different metal elements, can exhibit peculiar electronic, optical, and catalytic or photocatalytic properties that are absent in the corresponding monometallic nanoparticles. They are expected to display not only a combination of the properties associated with two distinct metals, but also new properties due to a synergy between two metals. The structure of bimetallic nanoparticles (BNPs) is defined by the distribution modes of the two elements and generally can be categorized into core-shell and alloy structures [1,2]. The effect of structure of Au/Pd bimetallic nanoparticles was estimated in catalytic reactions such as acetoxylation of ethylene to vinyl acetate [3], acetoxylation of toluene to benzylacetate [4], thrichloroethane hydrodechlorination [5] or organic compound oxidation [6–9]. Higher catalytic activity of Au(core)/Pd(shell) nanoparticles in comparison to alloy particles was reported for cyclohexane hydrogenation [10] and 4-nitrophenol reduction [11]. It was observed, that the nature and size distribution of the bimetallic nanoparticles is highly dependent upon both the heat treatment temperature, the composition of the atmosphere and type of support. Calcination of homogenous Au/Pd alloys immobilized at the Al_2O_3 surface, resulted in progressive enrichment of Pd at the metal particle surface and significant decrease in the activity of the catalyst [12]. On the other hand, Au(core)/Pd(shell) nanoparticles supported on a silica matrix have been transformed into a random alloy at 300 °C [10]. Au(core)/Pd(shell) nanoparticles supported on the TiO_2 were successfully prepared by a two step photodeposition method and have been applied to dechlorination of chlorobenzene under visible-light irradiation [13], while Au–Pd alloys immobilized on the TiO_2 surface have been synthesized via a sol-immobilization route and successfully used for phenol oxidation under UV light [14]. It was also found that the temperature employed in the calcination step (200, 300 and 400 °C) strongly influenced the reusability performance of the photocatalysts [14]. Recently it was shown that TiO_2 loaded with Ag/Au nanoparticles [15] or Pt/Pd [16] revealed a higher photoactivity in phenol degradation under visible light

* Corresponding author. Tel.: +48 58 347 24 37; fax: +48 58 347 20 65.
E-mail addresses: adriana.zaleska@pg.gda.pl, adriana.zaleska@ug.edu.pl (A. Zaleska).

0926-3373/$ – see front matter © 2014 Elsevier B.V. All rights reserved.
http://dx.doi.org/10.1016/j.apcatb.2014.01.042

than TiO_2 modified with monometallic nanoparticles, whilst the Au(core)/Ag(shell)–TiO_2 shown reduced photoactivity compared to TiO_2 with individual metal deposits [17]. Thus, the ability to control nanoscale alloying and phase segregation properties is important for the exploration of the bimetallic nanoparticles for the design of advanced catalysts, photocatalysts and other functional materials.

In view of this, we recently obtained TiO_2 loaded with Au/Pd nanoparticles using a microemulsion system of water, AOT (dioctyl sulfosuccinate sodium salt) and cyclohexane [15]. In this work we show the effect of calcination temperature (from 350 to 700 °C) on the structure and the photocatalytic properties of Au/Pd-modified TiO_2. For the first time, the composition of the bimetallic Au/Pd nanoparticles in relation to their photocatalytic performance as well as their ability to form radical species under UV and visible light as detected by EPR technique has been investigated.

2. Experimental

2.1. Materials and instruments

Titanium(IV) isopropoxide (TIP) (97%) was purchased from Aldrich Chem. and used as titanium source for the preparation of TiO_2 nanoparticles. $HAuCl_4$ (Au ~ 52%), $PdCl_2$ (5 wt% solution in 10 wt% HCl) from Sigma-Aldrich were used as metal source in the preparation procedure. Cyclohexane, isopropyl alcohol, sodium borohydride, hydrazine, acetone, AOT (dioctyl sulfosuccinate sodium salt) (POCH S.A. Poland) were used without further purification. Deionized water was used for all reactions and treatment processes. A commercial form of TiO_2 (P25, crystalline composition: 80% anatase, 20% rutile, surface area 50 g/m^2) from Evonik, Germany was used for the comparison of the photocatalytic activity.

Nitrogen adsorption–desorption isotherms were recorded at liquid nitrogen temperature (77 K) on a Micromeritics Gemini V (model 2365) and the specific surface areas were determined by the Brunauer–Emmett–Teller (BET) method in the relative pressure (p/p_0) range of 0.05–0.3. All the samples were degassed at 200 °C prior to nitrogen adsorption measurements. DRS UV–vis spectra of the synthesized materials were recorded in the scan range 200–900 nm using UV–vis spectrophotometer equipped with an integrating sphere and $BaSO_4$ was used as the reference. The photocatalyst powder crystal structure was determined from XRD pattern measured in the range of 2θ = 20–70° using X-ray diffractometer with Cu target $K\alpha$-ray (λ = 1.5404 Å). To determine particle sizes of the photocatalysts, XRD data were calculated using Scherrer's equation. X-ray photoelectron spectroscopy (XPS) experiments were performed in a PHI 5000 VersaProbe–Scanning ESCA Microprobe (ULVAC-PHI, Japan/USA) instrument at the base pressure below 5×10^{-9} mbar. X-ray beam was focused to diameter 100 μm, measured area was defined as 250 μm × 250 μm. A CasaXPS software was used to evaluate the XPS data (Shirley type background subtraction, quantification). For the final calibration of the spectra the peak Ti $2p_{3/2}$ of TiO_2 support was used with binding energy (BE) values = 458.60 eV.

X-band (ν = 9.5 MHz) EPR spectra were recorded by a Bruker EMX CW-microspectrometer at 90 K by the use of liquid nitrogen stream. An ER 4119HS-WI high-sensitivity optical resonator with a grid on the front side enabled irradiation of the sample by a 300 W Xe-arc lamp (LOT Oriel) equipped with an optical filter (GG 420). g values were calculated using the equation $h\nu = g\beta B_0$ with B_0 and ν being the resonance field and frequency, respectively. Calibration of the g values was performed using a DPPH standard (g = 2.0036 ± 0.00004).

2.2. Preparation of photocatalysts

Nanoparticles of titanium dioxide modified with Au and Pd were obtained by hydrolysis of TIP in the microemulsion system. Palladium precursor ($PdCl_2$) was added into water/AOT/cyclohexane microemulsion containing gold precursor ($HAuCl_4$) in water cores. The water content was controlled by fixing the molar ratio of water to the surfactant at 2 (*microemulsion* ***A***). Surfactant AOT was used as a stabilizer for the nanoparticles in the microemulsion system. Mixing of *microemulsion* ***A*** was carried out for 1 h under nitrogen and then gold and palladium were reduced by dropwise addition of *microemulsion* ***B*** containing the reducing agent (hydrazine or sodium borohydride). The molar ratio of the reducing agent to metal ions equaled 3. Then, the titanium(IV) isopropoxide was added into the microemulsion system containing gold and palladium nanoparticles. Obtained microemulsion was mixed and purged with nitrogen for 24 h and then obtained precipitate was washed with acetone and water to remove the remaining surfactant, dried at 80 °C for 48 h and calcined in air for 2 h at different temperatures. Unmodified TiO_2 which was the reference material, was received by the same method but without the addition of metal precursors.

2.3. Measurement of photocatalytic activity

The photocatalytic activity was estimated by measuring the decomposition rate of 0.21 mM phenol aqueous solution in the presence of visible and UV irradiation. The aqueous phase contained 125 mg of the photocatalyst, 24 cm^3 of deionized water and 1 cm^3 of phenol (Co = 500 mg/dm^3). The photocatalyst loading was 5 g/dm^3. The prepared suspension was stirred and aerated (V = 5 dm^3/h) for 30 min in the dark to obtained equilibrium and then the contents of the reactor was photoirradiated with a 1000 W Xenon lamp (Oriel) which emitted both UV and Vis irradiation. Measured light flux was (in the range from 310 to 380 nm) 62 mW/cm^2 for Xe lamp. The photoreactor (V = 25 cm^3) was equipped with a quartz window and exposure layer thickness was 3 cm. The optical path included a water filter and a glass filter (GG 420) which cut-off wavelengths shorter than 420 nm. The temperature of the aqueous phase during irradiation was kept at 10 °C using water bath. During the irradiation the suspension (1 cm^3) was collected, filtered through syringe filters (Ø = 0.2 μm) to remove the photocatalyst particles. Phenol concentration was estimated by colorimetric method (λ = 480 nm) after derivatization with diazo-*p*-nitroaniline using UV–vis spectrophotometer (DU-7, Beckman). Photocatalytic degradation runs were preceded by blind test in the absence of a photocatalysts or illumination. No degradation of phenol was observed in the absence of either the photocatalyst or illumination.

3. Results and discussion

In a typical reaction, the photodegration of phenol is performed in an aqueous phase under visible (λ > 420 nm) and UV–vis light irradiation. Initially, we investigated the effect of metal amount (Au to Pd ratio), as well as reducing agent type ($NaBH_4$ and N_2H_4) used during preparation route, on the photocatalytic activity of obtained Au/Pd–TiO_2 samples. The amount of gold and palladium precursors taken for photocatalyst preparation was calculated on the assumption that the content of Au and Pd in the photocatalysts after synthesis should be equal from 0.1 to 1.25 mol% of the photocatalyst dry mass. All the as-prepared TiO_2 samples loaded with Au–Pd nanoparticles, exhibited higher photoactivity than pure TiO_2 under visible and UV–vis irradiation (see Table 1). The Au/Pd–TiO_2 sample, prepared by using an Au/Pd ratio of 2.5 and hydrazine as a reducing agent, revealed the highest phenol degradation rate

Table 1
Sample label, preparation method and photoactivity of TiO_2 modified with gold and palladium nanoparticles—the effect of metal amount and reducing agent type.

Sample label	Amount of noble metal precursor [mol%] Pd	Au	Reducing agent	TiO_2 source[a]	Calcination temperature [°C]	BET surface area [m^2/g]	Phenol degradation rate under UV–vis [μmol/dm^3/min]	Phenol degradation rate under visible light [μmol/dm^3/min]
P25	0	0	0	$TiCl_4$	–	50	6.75	0.07
Pure/TiO_2_450	0	0	0	TIP	450	176	4.59	0.15
0.1Pd_$NaBH_4$/TiO_2_450	0	0.1	$NaBH_4$	TIP	450	167	6.77	1.35
0.1Pd_$NaBH_4$/TiO_2_400	0	0.1	$NaBH_4$	TIP	400	176	10.0	4.36
0.5Au_$NaBH_4$/TiO_2_450	0.5	0	$NaBH_4$	TIP	450	163	5.56	1.65
0.5Au_$NaBH_4$/TiO_2_400	0.5	0	$NaBH_4$	TIP	400	171	5.99	1.69
0.1Pd_1.25Au_N_2H_4/TiO_2_450	0.1	1.25	N_2H_4	TIP	450	179	6.03	0.54
0.1Pd_0.5Au_N_2H_4/TiO_2_450	0.1	0.5	N_2H_4	TIP	450	176	6.35	0.49
0.5Pd_1.25Au_$NaBH_4$/TiO_2_450	0.5	1.25	$NaBH_4$	TIP	450	186	6.00	0.42
0.5Pd_1.25Au_ N_2H_4/TiO_2_450	0.5	1.25	N_2H_4	TIP	450	186	6.19	0.82
0.5Pd_0.5Au_N_2H_4/TiO_2_450	0.5	0.5	N_2H_4	TIP	450	144	5.43	0.16
1Pd_1.25Au_$NaBH_4$/TiO_2_450	1	1.25	$NaBH_4$	TIP	450	182	6.62	0.43
1Pd_1.25Au_N_2H_4/TiO_2_450	1	1.25	N_2H_4	TIP	450	195	5.77	0.64
1Pd_0.5Au_N_2H_4/TiO_2_450	1	0.5	N_2H_4	TIP	450	171	5.61	0.73

under visible light among all photocatalysts modified with bimetallic Au/Pd nanoparticles (0.82 μmol/dm^3/min) and this sample was chosen to investigate the effect of calcination temperature on the structure of the Au–Pd bimetallic nanoparticles.

3.1. Morphology

The composition of the bimetallic NPs located at the TiO_2 surface was studied using Cs-corrected STEM (High Angle Annular Dark Field, HAADF) imaging supplemented with EDXS mapping as shown in Fig. 1. Therefore it is possible to get images in high resolution with *z*-contrast based on the elastic scattering of the primary beam with the sample. This is an advantage especially in the case of small and very small particles of heavy elements to detect their internal structures like core/shell structures, fluctuations in composition within particles and so on which are often not visible in conventional TEM. The differences in contrast shown in 1b are generated by the composition and not by thickness. Bright for Au while less bright for Pd since it is the smaller atom. Thus, regions circled in yellow in Fig. 1b show gold-rich areas by contrast. The check by the color distribution of the EDXS maps and single measurements at different areas within one particle (not shown here) confirmed this result. The diameters of the observed Au/Pd nanoparticles varied from about 5 to 300 nm depending on calcination temperature. Fig. 1 shows typical examples of these particles at different temperatures. This points to a good interaction between the Au/Pd particles and the TiO_2 surface in the microemulsion preparation method, however it also indicated that microemulsion system don't promote formation of particles with narrow size distribution. For the 350 C sample, three main fractions of Au/Pd nanoparticles could be distinguished: (a) small spherical particles in the range of 1 to 6 nm; (b) particles with anisotropic shapes differing from 15 to 50 nm (biggest observed), and (c) spherical (about 50 nm). Sample calcinated at 400 C had small spherical nanoparticles in the range of 4 to 10 nm and bigger, anisotropic in the shape, particles in the range from 15 to 115 nm (biggest observed). For sample treated at 450 °C, no particles smaller than 10 nm was found. Au/Pd particles in the range from 10 to 50 nm were spherical, since bigger once (from 70 to 360 nm) had anisotropic shape. Calcination at 700 °C resulted in formation of mostly anisotropic 15–20 nm particles together with anisotropic 65–330 nm particles.

In case of the sample calcined at 350 °C, it could be observed that the core of bimetallic NPs was rich in gold, however the shell contained mostly palladium. The average Pd/Au ratio changed from 1:4 in the core region to 5:1 in the surface layer. Rising the calcination temperature from 350 to 700 °C led to alloying of the metals and increased the size of nanoparticles. The internal structure of the nanoparticles changed from core shell structures to island like structures with areas of different compositions and ends at 700 °C in a fully alloyed system. For surface compositions this change it can be expected that within this process the Pd content decreases while more Au reaches the surface till the composition of the complete alloy is reached at 700°. The Pd/Au ratio varied in different nanoparticle regions, but the EDX spectra clearly indicated that the gold content is higher than palladium content both in core and shell regions for all samples calcined at 450 °C and above. Thus, the increase of calcination temperature caused a re-distribution and segregation of the metal particles at the TiO_2 surface and EDX results indicate that that the shell region is enriched in gold with an increase of temperature. Segregation of the bimetallic nanoparticles during thermal treatment was previously observed for Au/Pt system by Wanjala et al. [18]. As-prepared Au/Pd–TiO_2 samples were obtained by adding palladium ions to microemulsions containing gold ions in the internal phase (water droplets of microemulsion system). Regarding different redox potentials of these metals (Au^{3+}/Au: 1.41 V; Pd^{2+}/Pd: 0.99 V in aqueous solution

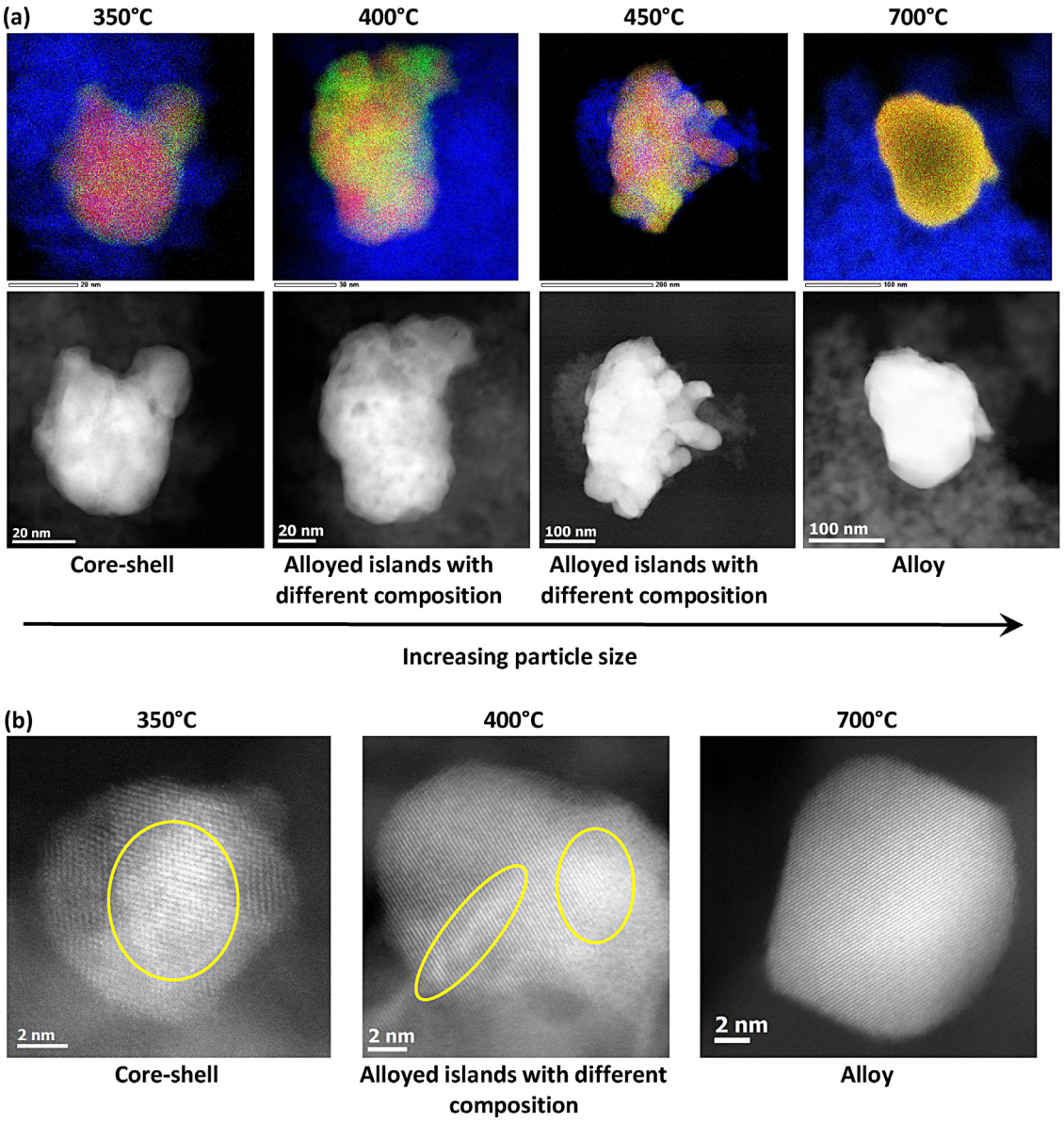

Fig. 1. HAADF images combined with mappings of palladium–gold–titania (blue is Ti, red is Au and green Pd) calcined at 350, 400, 450 and 700 °C (a) and high resolution HAADF images with *z*-contrast for Au/Pd nanoparticles calcined at 350, 400 and 700 °C (b). The yellow circles show gold-rich areas (palladium gives a light contrast than gold as a lighter element) (For interpretation of the references to color in this figure legend, the reader is referred to the web version of this article.).

at 25 °C [19]), gold is more easily reduced and provides a seed for the reduction of the palladium-enriched shell [20,21]. After addition of the reducing agent, Pd ions located around cathodically polarized (double-layer-charging) Au nanoparticles, were reduced at the gold surface and formed a Pd-rich shell (see Fig. 2). On the other hand, Au has a lower surface free energy (1.626 J/m^2) than Pd (2.043 J/m^2) [3] and the elements with lower surface energy tend to segregate to the surface [1,18]. This difference favors the formation of Au shell and therefore partial phase segregation of Au at the surface was observed in the Au/Pd system with increase of calcination

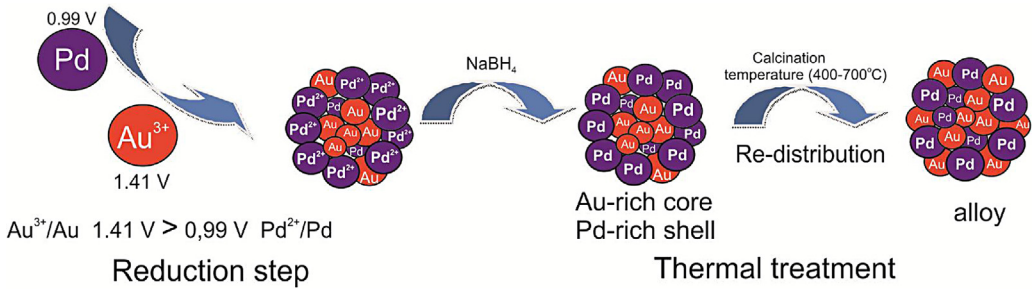

Fig. 2. Formation of Au/Pd nanoparticles at the TiO_2 surface during synthesis in the microemulsion system and further thermal treatment.

temperature. At calcination temperatures above 400 °C it was observed that the gold content enriched in the region near the outer shell, whereas the palladium concentration enriched in the core region.

3.2. UV–vis properties and BET surface area

Fig. 3 shows DRS spectra of pure TiO_2, TiO_2 modified with Au, Pd or Au/Pd nanoparticles (Fig. 3a) and 0.5Pd_1.25Au/TiO_2 calcined at different temperature (from 350 to 700 °C) (Fig. 3b). For samples containing only Au, the characteristic surface plasmon resonance (SPR) band maximum is observed at about 560 nm, which is in good agreement with the intristic interband transition around 2.5 eV for Au nanoparticles [22]. In case of Pd, the d-band overlaps with the s- and p-bands in the whole range of interest, leading to broad optical resonances that have been assigned to so-called localized surface plasmon resonances (LSPRs) [23]. Overlaping interband continuum with the plasmon resonance for Pd nanoparticles results in approximately uniform background Characteristic SPR absorption of gold was also evident in the case of Au/Pd bimetallic nanoparticles, since these particles contain gold in excess (Au:Pd = 12.5:1), while for samples with higher palladium to gold ration (Au:Pd = 2.5:1) plasmonic band is suppressed. Quite wide absorption band could be related to wide size distribution of Au/Pd particles deposited at the TiO_2 surface. The position and shape of plasmonic band is dependent on the size of metallic nanoparticles. LSPR can be tuned from the near-UV through the visible region and even into the mid-IR by changing the size and shape of the nanoparticles [24–26]. Kowalska et al. observed that Au@TiO_2 powders with different sizes of gold (from 10 to 100 nm) deposited on TiO_2 surface showed localized surface plasmon resonance (LSPR) in visible region with broad absorption band in the wavelength range around 400–700 nm [25]. The rod-like gold nanoparticles exhibited longitudinal (ca. 600 nm) and transverse (ca. 520 nm) LSPR, while absorption of nano-size gold spherical particles was observed for much shorter wavelengths [17].

The Au/Pd–TiO_2 sample without calcination had the highest BET surface area of about 288 m^2/g (see Table 2). As the calcination temperature increased, the BET surface area of Au/Pd–TiO_2 decreased progressively and fluctuated from 225 to 59 m^2/g, due to sintering and crystal growth of TiO_2 particles [27].

3.3. XRD analysis

The effect of calcination temperature on the TiO_2 crystal structure and bimetallic nanoparticles structure was evaluated using XRD analysis (shown in Fig. 4). Typical diffraction peaks corresponding to anatase (2θ = 25°, 48°, 55°) were observed in all the samples and the intensity of the peaks increased with the increase of temperature. For the samples calcined from 350 to 600 °C we observed peaks originating from the brookite phase. At 700 °C weak reflections attributed to rutile appeared. The presence of a broad peak in the diffractograms of the bimetallic samples, centered at a value intermediate between the (1 1 1) peaks of metallic gold (2θ = 38.2°, 44.4°) and metallic palladium (2θ = 40.1°, 46.7°) is an indication of alloy formation [28]. The diffraction peaks of 38.3° and 44.2° could be attributed to a gold-enriched alloy phase and the peaks of 40.2° and 46.4° to a palladium-enriched alloy phase. As expected, with increasing calcination temperature we observed bigger crystallite sizes (from 25 to 63 nm).

3.4. Composition of Au/Pd–TiO_2

The surface atomic compositions of Au/Pd–TiO_2 calcined at 350–700 °C were estimated by XPS analysis and are shown in Tables 3 and 4. The titanium peaks are located at binding energies

Table 2
Sample label, preparation method and photoactivity of Au/Pd–TiO_2 samples calcinated from 350 to 700 °C.

Sample label	Amount of noble metal precursor (mol%)		Reducing agent	TiO_2 source[a]	Calcination temperature (°C)	BET surface area (m^2/g)	Phenol degradation rate under (μmol/dm^3/min)		Element content (mas%)		
	Pd	Au					UV–vis	visible light (λ > 420 nm)	C	H	S
Pd_Au/TiO_2	0.5	1.25	N_2H_4	TIP	not treated	288	–	–	15.34	3.39	2.01
Pd_Au/TiO_2_350	0.5	1.25	N_2H_4	TIP	350	225	5.8	3.8	0.88	0.32	1.49
Pd_Au/TiO_2_400	0.5	1.25	N_2H_4	TIP	400	198	7.1	3.4	0.14	0.48	1.45
Pd_Au/TiO_2_450	0.5	1.25	N_2H_4	TIP	450	186	6.2	0.8	0.24	0.31	1.53
Pd_Au/TiO_2_500	0.5	1.25	N_2H_4	TIP	500	166	7.3	1.1	0.07	0.17	1.36
Pd_Au/TiO_2_600	0.5	1.25	N_2H_4	TIP	600	104	5.6	0.5	0.07	0.14	1.21
Pd_Au/TiO_2_700	0.5	1.25	N_2H_4	TIP	700	59	5.7	0.7	0.1	0.05	0.23

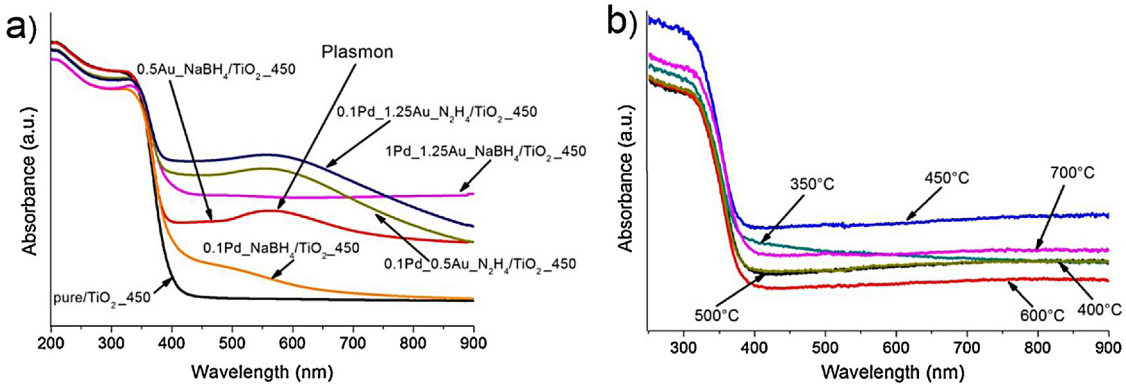

Fig. 3. DRS spectra of pure TiO_2 and TiO_2 modified with monometallic and bimetallic nanoparticles (different ratio of Au:Pd) (a), and samples 0.5Pd_1.25Au/TiO_2 calcined at temperature from 350 to 700 °C (b).

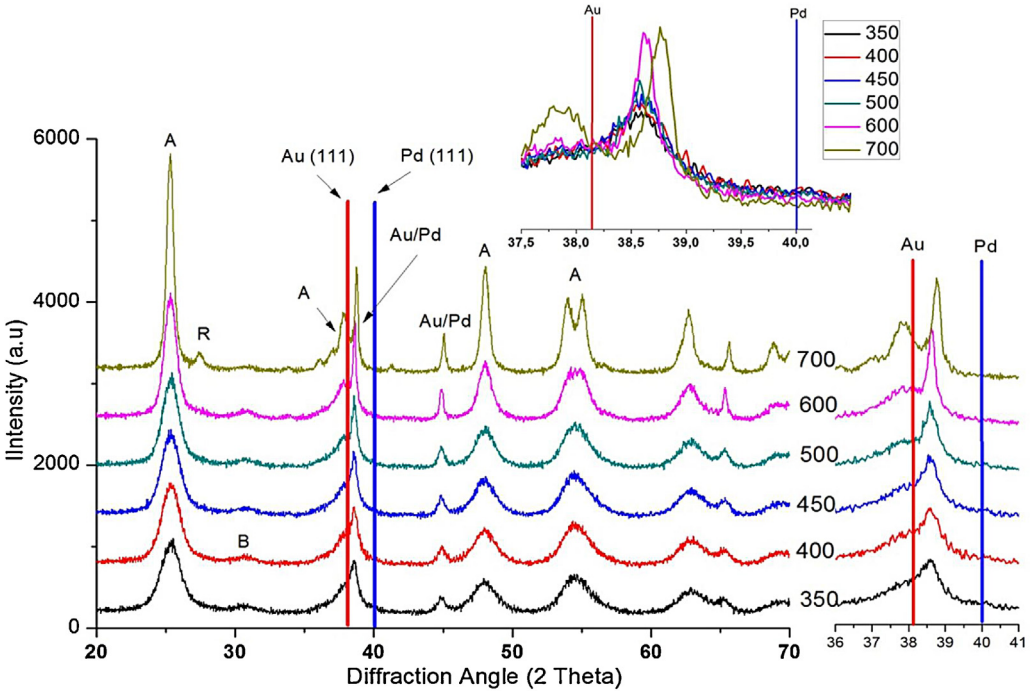

Fig. 4. XRD pattern of sample the Pd/Au-TiO_2 samples calcinated from 350 to 700 °C.

Table 3
Au/Pd–TiO_2 surface composition—the effect of calcination temperatures.

Sample label	Ti content (at%)	O content (at%)	C content (at%)	Au content (at%)	Pd content (at%)	Fraction Pd state %		Impurities (at%)
						Pd $3d_{5/2}$		
						Pd^0 334.7 ± 0.3 eV	Pd^{2+} 336.8 ± 0.4 eV	
Pd_Au/TiO_2 _350	20.0	59.9	17.3	0.05	0.08	44.5	55,5	2.7
Pd_Au/TiO_2 _400	23.7	62.9	10.7	0.07	0.08	39.2	60.8	2.6
Pd_Au/TiO_2 _450	22.2	64.7	12.2	0.05	0.07	29.5	70.5	0.8
Pd_Au/TiO_2 _500	23.1	64.8	11.0	0.07	0.07	19.1	80.9	1.0
Pd_Au/TiO_2 _600	23.5	63.9	11.5	0.06	0.12	13.5	86.5	1.0
Pd_Au/TiO_2 _700	24.7	59.6	14.3	0.06	0.09	24.6	75.4	1.2

Table 4
Chemical character and amount of Ti, O and C atoms incorporated into surface layer of the Au/Pd–TiO_2 samples calcinated from 350 to 700 °C.

Sample label	$\%Ti^{+4}$	$\%Ti^{+3}$	$\%>O^{2-}$	%Ti–OH/C–OH	%C=O	%C–C/C–H	%C–OH	%C=O	%COOH
	458.60 eV	457.1 ± 0.25 eV	529.85 ± 0.02 eV	531.1 ± 0.2 eV	532.2 ± 0.2 eV	284.5 ± 0.2 eV	286.1 ± 0.2 eV	287.3 ± 0.2 eV	288.9 ± 0.2 eV
Pd_Au/TiO_2 _350	98.1	1.9	65.7	21.3	13.0	51.8	29.5	8.4	10.3
Pd_Au/TiO_2 _400	98.3	1.7	74.6	17.0	8.4	58.2	20.5	11.8	9.5
Pd_Au/TiO_2 _450	99.4	0.6	71.3	16.6	12.0	30.6	50.6	13.4	5.4
Pd_Au/TiO_2 _500	98.8	1.2	74.7	16.0	9.3	48.5	36.2	9.6	5.7
Pd_Au/TiO_2 _600	98.5	1.5	78.2	14.0	7.8	60.9	26.5	6.2	6.5
Pd_Au/TiO_2 _700	96.9	3.1	71.8	16.3	11.9	54.9	21.7	11.5	11.9

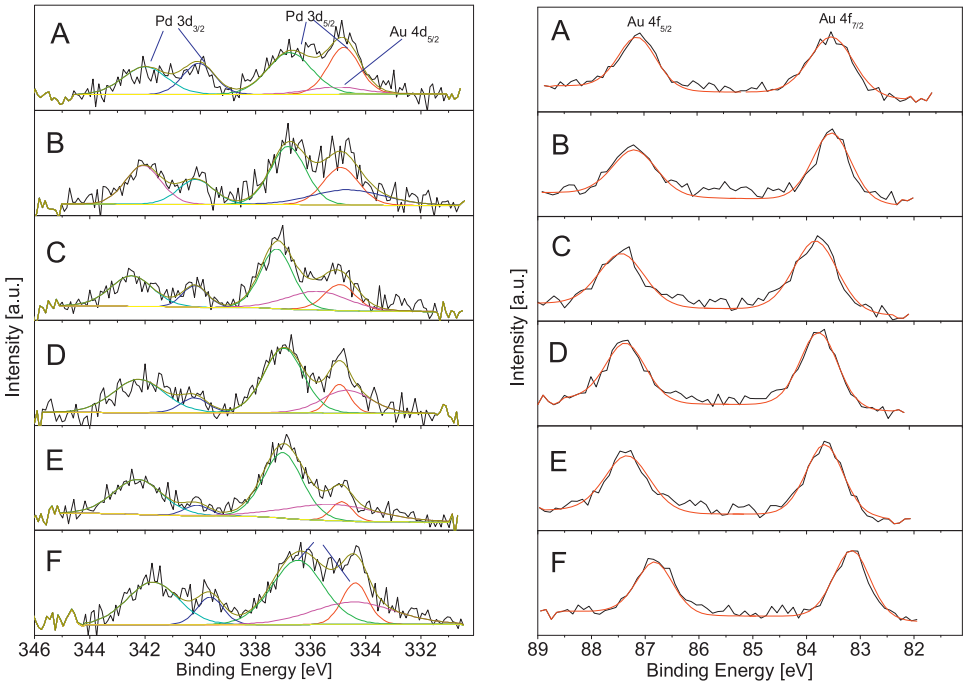

Fig. 5. XPS spectra of the 0.5Pd_1.25Au_TiO_2 calcined at different temperatures: (a) 350 °C (b) 400 °C, (c) 450 °C, (d) 500 °C, (e) 600 °C, (f) 700 °C.

~458.6 (Ti $2p_{3/2}$) and ~464.4 eV (Ti $2p_{1/2}$) [29]. The strong peak at 458.6 indicates that the Ti^{4+} is the dominant surface state [27]. The Ti content was the smallest for the sample calcined at 350 °C. Three peaks O 1s composed of different species, were identified (C–O–H, Ti–O–H or/and C–O–H and C=O). XPS analysis enabled detection of carbonaceous species on the Au/Pd–TiO_2 surface as C–C, C=O, C–OH and –COOH peaks, which appeared from 285 to 289.6 eV. The carbon content on the surface of the Au/Pd–TiO_2 photocatalysts varied from 10.7 to 17.3 at% and originated from the surfactant, the TiO_2 precursor, the reducing agent and the oil phase. According to literature, the activity of photocatalysts under visible light could be enhanced by the presence of carbonaceous species (C–C) occurring in a highly condensed and coke-like structure, which could play the role of a sensitizer to induce visible light absorption and response [30,31]. We also observed a small amount of sulfur in all the samples. It originated from surfactants used during preparation route.

The gold content on the surface differed from 0.05 to 0.07 at% (Table 3). The Au $4f_{7/2}$ and Au $4f_{5/2}$ binding energy peaks for generally appeared at 83.2–83.7 eV. All E_B values of Au $4f_{7/2}$ were significantly lower than that of bulk gold. This negative shift of BE could be caused by electron transfer from Pd [32] or from TiO_2 [32,33]. Based on this, it is deduced that gold in 1.25Au_0.5Pd/TiO_2 photocatalysts exists mainly in a metallic alloy state but the existence of small cluster $Au^{\delta-}$ is also possible. The palladium content on the surface differed from 0.08 to 0.12 at%. The peaks were observed at a binding energy of 334.4–335.0 and ~336.5–337.2 eV, corresponding to the Pd $3d_{5/2}$ peak in the alloy and in PdO, respectively (see Fig. 5) The Pd $3d_{5/2}$ and $3d_{3/2}$ peaks were shifted to lower energy by about 1 eV compared to pure bulk Pd metal (335 eV) [28,34]. As the calcination temperature increased, the peaks at 334.8 and 340.0 eV (Pd^0) decreased gradually while the peaks at 336.8 and 342.0 eV (Pd^{2+}) increased. This peak shift might be ascribed to the interaction between the Pd nanoparticles and TiO_2. Some researchers described that the lower E_B value of Pd 3d might be due to the gain of charge density in the d band, concomitant with the loss in the sp band, suggesting a more pronounced Au–Pd bond formation on the surface of AuPd nanoparticles [32]. To gain insight into the structure of the photocatalyst, ICP–AES analysis of the 1.25Au_0.5Pd/TiO_2 calcined at 450 °C was performed. Au and Pd contents of 1.72 and 0.53 at%, respectively, were found. According to the XPS data, the Au and Pd contents on the 1.25Au_0.5Pd/TiO_2 surface calcined at 450 °C equaled to only 0.05 and 0.07 at%, respectively (see Table 5). These results show that the majority of metal nanoparticles Au and Pd are located underneath the TiO_2 surface due to subsequent formation of TiO_2 and metallic nanoparticles in the microemulsion system.

The carbon content in the Au/Pd–TiO_2 photocatalysts was additionally confirmed by elemental analysis (see details in Table 2) and it varied from 0.07% to 15.34%, depending on the calcination temperature. As expected, the highest amount of carbon was observed for the uncalcined sample (15.34%). With increasing calcination temperature, the content of C, H and S originating from reagents used during synthesis, decreased.

3.5. Photocatalytic activity

Generally, it was observed, that in case of Au/Pd–TiO_2 nanoparticles, enhancement of calcination temperature from 350 to 700 °C resulted in a slight drop of photoactivity under UV and quite rapid drop under visible light (see Table 2 and Fig. 6a and b). When the calcination temperature was elevated from 350 °C, the UV-mediated photoactivity increased. The phenol degradation rate increased from 5.8 to 7.1 and 6.2 μmol/dm^3/min for photocatalyst calcined at 350, 400 and 450 °C, respectively. The highest photoactivity under UV light was observed for the sample calcined at 500 °C. Further increase in annealing temperature resulted in a drop of photoactivity to 5.7 μmol/dm^3/min for the sample calcined at 700 °C. On the other hand, the visible light activity was suppressed for samples treated at higher temperature. Thus, the phenol degradation rate under visible light decreased from 3.8 and 3.4 μmol/dm^3/min for the sample calcined at 350 and 400 °C, respectively, to 0.7 μmol/dm^3/min after calcination at 700 °C. The samples calcined at 350 and 400 °C have much higher activity than those calcined from 450 to 700 °C.

Table 5
Quantified XPS and ICP-AES data for the bimetallic nanoparticles (sample calcinated at the 450 °C).

Photocatalyst	ICP-AES		XPS	
	Au content (at%)	Pd content (at%)	Au content (at%)	Pd content (at%)
Pd_Au/TiO_2	1.72	0.53	0.05	0.07

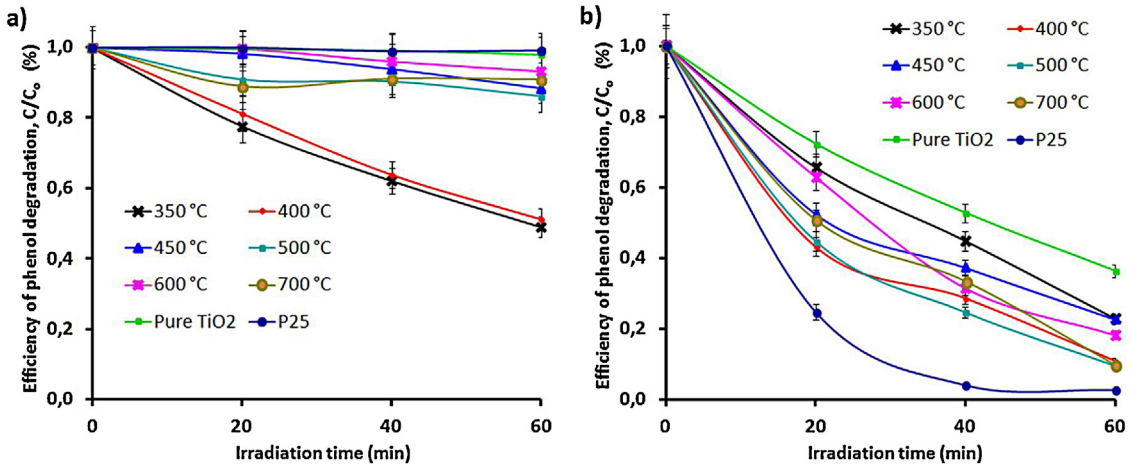

Fig. 6. Kinetics of phenol degradation for sample 0.5Pd_1.25Au_TiO_2 calcined at different temperatures: (a) under visible light, and (b) under UV–vis light. Experimental conditions: light source: Xe lamp, λ > 420 nm, phenol initial concentration: 0.21 mM, m(TiO_2) = 125 mg, T = 10 °C.

3.6. In-situ EPR spectroscopy

In situ EPR spectroscopy was used to examine the relevance of paramagnetic species formation under visible (vis) as well as under UV–vis light excitation for the activity of the 1.25Au_0.5Pd/TiO_2 photocatalysts in phenol degradation calcined at different temperatures. In situ EPR spectra were recorded starting in the dark followed by subsequent irradiation, first with pure visible light (λ > 420 nm) and then using UV–vis light by removing the optical filter. Fig. 7 shows the difference EPR spectra of all Au/Pd–TiO_2 samples obtained by subtracting the dark spectrum from the one after 10 minutes of visible light irradiation (black lines). To visualize the spectrum changes by the addition of UV light, the spectrum under visible light was subtracted from the one after further 10 minutes of UV–vis irradiation (gray lines). Visible light irradiation led to the formation of an isotropic signal at g = 2.0038 for the samples calcined until 450 °C (signal **C** in Fig. 7), which was not observed for pure TiO_2. This signal might arise from radical species deriving from carbon residues as described above. Although the uncalcined sample exhibits the highest carbon content, the carbon radical signal **C** is only very low in such hydroxylated samples. Here, besides a weak carbon radical line **C** under visible light excitation, typical EPR signals of $H_2O\bullet$ (signal **A**) and Ti^{3+} within anatase (signal **B**) were observed only under UV–vis light (see Table 6) [35–38]. As described above, it was reported earlier that the intensity of signal **C** and thus the number of organic radical species might correlate with the visible light photocatalytic activity in the degradation of organic compounds [37]. Therefore, the high signal **C** intensity for the samples calcined at 350 and 400 °C could explain their good visible light photoactivity. Under UV–vis light irradiation, $O^{\bullet-}$ radicals were formed by trapping the photo-generated positive holes in the valence band at subsurface (O_B^-, signal **D**) and surface (O_S^-, signal **E**) lattice oxygen ions. Interestingly, the amount of bulk-like oxygen radicals (signal **D**) seems to decrease with higher calcination temperature while the O_S^- signal intensity increases, probably due to less carbon-capping. Herein, it was further observed that the subsurface O_B^- species is even stable after turning off the light (in the samples calcined until 500 °C), while the signal **E**

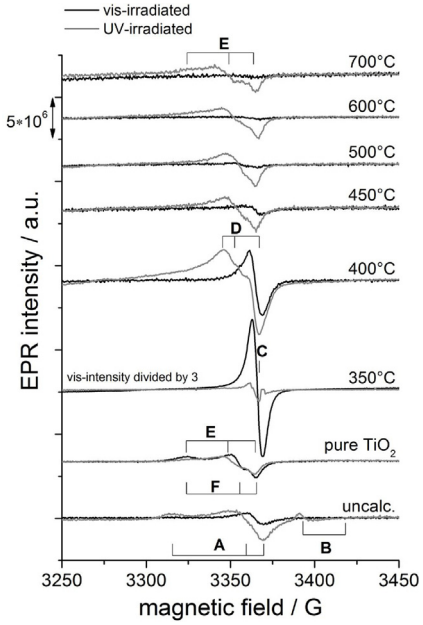

Fig. 7. EPR difference spectra of TiO_2 loaded with 1.25Au and 0.5Pd and calcined at different temperatures from 350 to 700 °C. Black lines: spectrum in the dark subtracted from spectrum under visible light, grey lines: spectrum under visible light subtracted from spectrum under UV–vis irradiation.

Table 6
EPR parameters of detected signals and their assignment based on literature data.

Signal	g_1	g_2	g_3	Assignment
A	2.035	2.009	2.002	Ti^{4+}–O_2H [30]
B	1.989	1.958		Ti^{3+} in anatase [31]
C	2.003			carbon-radical [32,33]
D	2.018	2.014	2.004	Ti^{4+}–O^-–Ti^{4+}–OH^- (O_B^-) [30]
E	2.028	2.015	2.003	Ti^{4+}–O^{2-}–Ti^{4+}–O^- (O_s^-) [34]
F	2.028	2.010	2.004	Ti^{4+}–O_2H [35]

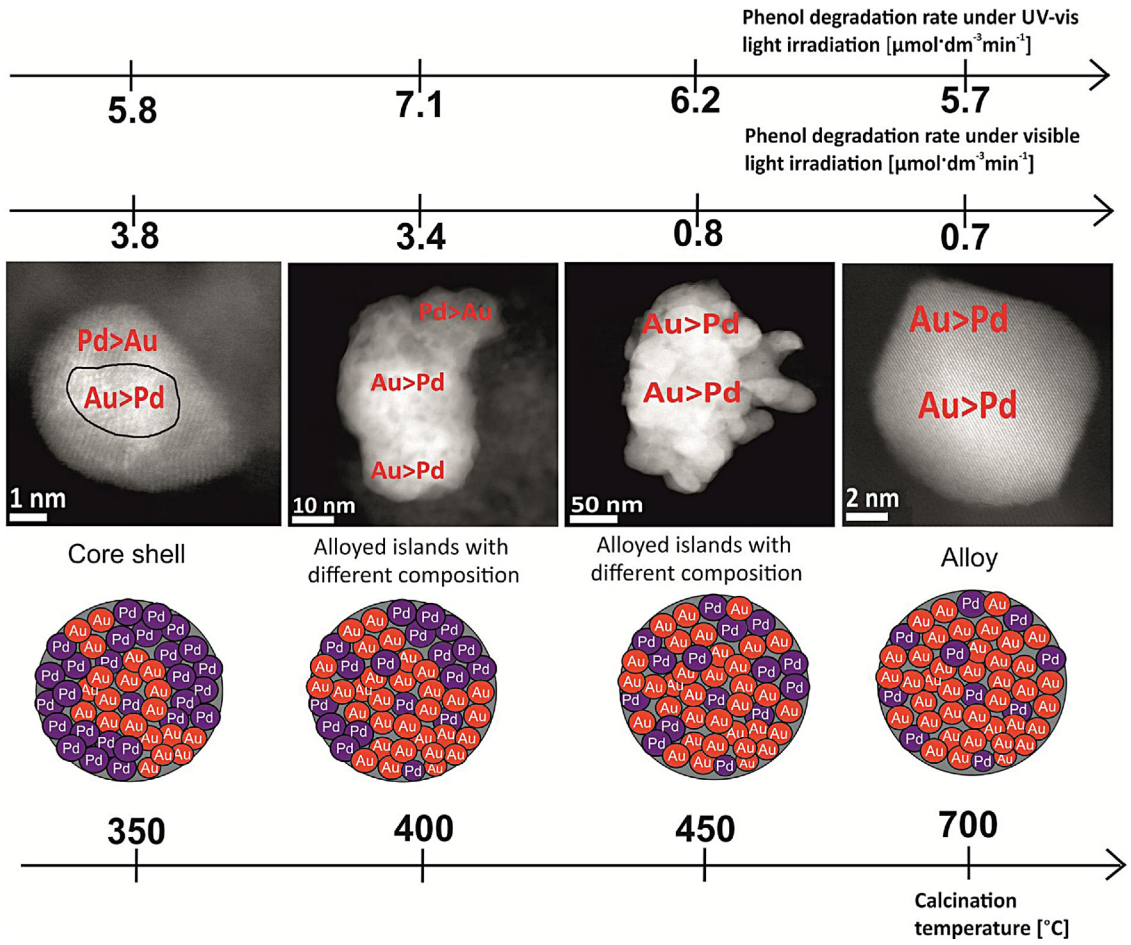

Fig. 8. The effect of calcination temperature on the structure of Au/Pd bimetallic nanoparticles and photoactivity of Au/Pd–TiO_2 nanocomposites.

intensity vanishes quickly even under further irradiation, as observed for the sample calcined at 700 °C. EPR results are in good agreement with photoactivity in phenol degradation reaction under UV and visible light. Most intensive EPR signals are observed for samples showing highest photoactivity.

Increasing treatment temperature leads to a shrinking of the surface area and structure changes of TiO_2 together with phase segregation of the bimetallic Au/Pd nanoparticles, which finally results in the loss of activity, especially under visible light. The observed drop in visible light photoactivity could be related to a phase segregation of the bimetallic Au/Pd nanoparticles as well as decrease of carbon content in TiO_2 matrix, although we did not observe a correlation between carbon content on the surface and visible photoactivity. However, the photocatalysts containing more carbon species clearly showed better activity, which is in good agreement with our previous results [27]. The highest carbon amount on the surface was observed for the photocatalyst calcined at 350 °C, and this sample exhibited the highest activity under visible light.

The Au/Pd–TiO_2 sample calcined at 350 °C which showed the highest activity under visible irradiation contained the highest carbon content (among all the calcined samples) and the highest Pd/Au ratio on the surface of metal particle surface. The decrease of palladium concentration in the outer shell resulted in lower visible light photocatalytic activity, as shown in Fig. 8. Only TiO_2 samples modified with Au/Pd nanoparticles enriched in palladium in the shell region (Pd to Au ratio from 5:1 to 2:1) show visible light response in phenol degradation reaction. This agrees well with the fact that lower photocatalytic activity has been observed for pure Au–TiO_2 compared to pure Pd–TiO_2. This conclusion is also consistent with the fact that gold and palladium nanoparticles revealed different plasmonic properties. Localized surface plasmon resonance (LSPR) means collective oscillations of conduction electrons trapped at metal–dielectric interfaces. The frequency of the LSPR can be tuned by changing size, shape, and dielectric environment of the particles. Once excited, a LSPR can decay radiatively by re-emission of a photon ("scattering"), or nonradiatively ("absorption") via electron–hole pair formation [39]. It was reported by Langhammer et al. [39] that for Pd nanoparticles the nonradiative decay of the LSPR is the dominant decay channel. For Au nanoparticles with a diameter of about 20–40 nm the radiative decay dominates and thus fewer e^-h^+ pairs are created via LSPR decay in Au, despite an overall larger total extinction, compared to Pd. The dominance of the absorption channel in Pd nanoparticles together with the tuning ability of the LSPR makes them suitable candidates for e^-h^+ transfer to HOMO and LUMO resonances of molecules and particles adsorbed on the Pd nanoparticles [21].

4. Conclusions

In summary, the calcination temperature affected both: the structure of Au/Pd nanoparticles as well as crystal structure and surface properties of TiO_2 support. In the TiO_2 matrix, increasing calcination temperature causes a surface area shrinking, growth of crystal size, slight transformation from anatase to rutile phase and change in content and chemical character of carbon incorporated in surface layer. Au/Pd bimetallic nanoparticles formed at the TiO_2 surface in the microemulsion system have an Au-rich core and a Pd-rich shell. Increasing temperature from 350

to 700 °C during calcination step, causes gold-enrichment in the surface region. UV-initiated activity of Au/Pd–TiO_2 photocatalysts decreases only slightly with enhancement of calcination temperature. Based on EPR spectra, it seems that formation of $O^{\bullet-}$ radicals is mainly responsible for phenol degradation under UV light for all Au/Pd–TiO_2 samples. However, the amount of bulk-like oxygen radicals decreases with higher calcination temperature while the amount of surface-like oxygen radicals increases, probably due to less carbon-capping. Thus, Au/Pd nanoparticles deposited at the TiO_2 surface worked as an electron trap, facilitate electron–hole separation and promote the interfacial electron transfer process. The most probable pathway of phenol degradation under UV light is direct reaction with oxygen radicals and additional direct charge transfer to adsorbed compound.

Visible light initiated activity in phenol degradation reaction was observed only for Au/Pd–TiO_2 samples calcinated at 350 and 400 °C. Further metal re-distribution, observed upon increasing temperature from 450 to 700 °C causes gold-enrichment in the surface region of Au/Pd nanoparticles, finally leading to visible light photoactivity decrease due to weaker ability of charge carriers formation during excitation of gold, compared to palladium. Thus, palladium presence at the surface of Au/Pd nanoparticles seated on TiO_2 is more favorable from the photocatalytic point of view than gold presence.

Acknowledgment

This research was financially supported by National Centre for Research and Development (strategic program: Advanced Technologies for Energy Generation. Task 4: Elaboration of Integrated Technologies for the Production of Fuels and Energy from Biomass, Agricultural Waste and other Waste).

References

[1] R. Ferrando, J. Jellinek, R.L. Johnston, Chemical Reviews 108 (2008) 845–910.
[2] R. Ghosh Chaudhuri, S. Paria, Chemical Reviews 112 (2011) 2373–2433.
[3] M. Chen, D. Goodman, Chinese Journal of Catalysis 29 (2008) 1178–1186.
[4] G. Suresh, J. Radnik, V.N. Kalevaru, M.-M. Pohl, M. Schneider, B. Lücke, A. Martin, N. Madaan, A. Brückner, Physical Chemistry Chemical Physics 12 (2010) 4833–4842.
[5] L.A. Pretzer, H.J. Song, Y.-L. Fang, Z. Zhao, N. Guo, T. Wu, I. Arslan, J.T. Miller, M.S. Wong, Journal of Catalysis 298 (2013) 206–217.
[6] A. Villa, N. Janjic, P. Spontoni, D. Wang, D.S. Su, L. Prati, Applied Catalysis A: General 364 (2009) 221–228.
[7] M.I. bin Saiman, G.L. Brett, R. Tiruvalam, M.M. Forde, K. Sharples, A. Thetford, R.L. Jenkins, N. Dimitratos, J.A. Lopez-Sanchez, D.M. Murphy, Angewandte Chemie International Edition 51 (2012) 5981–5985.
[8] E. Cao, M. Sankar, E. Nowicka, Q. He, M. Morad, P.J. Miedziak, S.H. Taylor, D.W. Knight, D. Bethell, C.J. Kiely, A. Gavriilidis, G.J. Hutchings, Catalysis Today 203 (2013) 146–152.
[9] M. Hosseini, T. Barakat, R. Cousin, A. Aboukaïs, B.L. Su, G. De Weireld, S. Siffert, Applied Catalysis B: Environmental 111–112 (2012) 218–224.
[10] T. Nakagawa, H. Nitani, S. Tanabe, K. Okitsu, S. Seino, Y. Mizukoshi, T.A. Yamamoto, Ultrasonics Sonochemistry 12 (2005) 249–254.
[11] P. Venkatesan, J. Santhanalakshmi, Nanoscience and Nanotechnology 1 (2011) 43–47.
[12] A. Herzing, A. Carley, J. Edwards, G. Hutchings, C. Kiely, Chemistry of Materials 20 (2008) 1492–1501.
[13] A. Tanaka, K. Fuku, T. Nishi, K. Hashimoto, H. Kominami, The Journal of Physical Chemistry C 117 (2013) 16983–16989.
[14] R. Su, R. Tiruvalam, Q. He, N. Dimitratos, L. Kesavan, C. Hammond, J.A. Lopez-Sanchez, R. Bechstein, C.J. Kiely, G.J. Hutchings, ACS Nano 6 (2012) 6284–6292.
[15] A. Zielińska-Jurek, E. Kowalska, J.W. Sobczak, W. Lisowski, B. Ohtani, A. Zaleska, Applied Catalysis B: Environmental 101 (2011) 504–514.
[16] A. Zielińska-Jurek, J. Hupka, Catalysis Today (2013), http://dx.doi.org/10.1016/j.cattod.2013.11.044.
[17] E. Kowalska, M. Janczarek, L. Rosa, S. Janczarek, L. Rosa, S. Juodkazis, B. Ohtani, Catalysis Today (2013), http://dx.doi.org/10.1016/j.cattod.2013.11.021.
[18] B.N. Wanjala, J. Luo, B. Fang, D. Mott, C.-J. Zhong, Journal of Materials Chemistry 21 (2011) 4012–4020.
[19] G.H. Aylward, T.J.V. Findlay, SI Chemical Data, 4th ed., Wiley, 1999.
[20] C. Kan, W. Cai, C. Li, L. Zhang, H. Hofmeister, Journal of Physics D: Applied Physics 36 (2003) 1609.
[21] M.R. Knecht, M.G. Weir, A.I. Frenkel, R.M. Crooks, Chemistry of Materials 20 (2007) 1019–1028.
[22] H. Gao, J. McMahon, M. Lee, J. Henzie, S. Gray, G. Schatz, T. Odom, Optics Express 17 (2009) 2334–2340.
[23] T. Pakizeh, C. Langhammer, I. Zoric, P. Apell, M. Käll, Nano Letters 9 (2009) 882–886.
[24] E. Kowalska, R. Abe, B. Ohtani, Chemical Communications (2009) 241–243.
[25] E. Kowalska, O.O.P. Mahaney, R. Abe, B. Ohtani, Physical Chemistry Chemical Physics 12 (2010) 2344–2355.
[26] Y. Xia, N.J. Halas, MRS Bulletin 30 (2005) 338–348.
[27] P. Górska, A. Zaleska, E. Kowalska, T. Klimczuk, J.W. Sobczak, E. Skwarek, W. Janusz, J. Hupka, Applied Catalysis B: Environmental 84 (2008) 440–447.
[28] A.M. Venezia, V. La Parola, G. Deganello, B. Pawelec, J.L.G. Fierro, Journal of Catalysis 215 (2003) 317–325.
[29] M.E. Simonsen, H. Jensen, Z. Li, E.G. Søgaard, Journal of Photochemistry and Photobiology A: Chemistry 200 (2008) 192–200.
[30] A. Zaleska, E. Grabowska, J.W. Sobczak, M. Gazda, J. Hupka, Applied Catalysis B: Environmental 89 (2009) 469–475.
[31] S. Sakthivel, H. Kisch, Angewandte Chemie International Edition 42 (2003) 4908–4911.
[32] A. Murugadoss, K. Okumura, H. Sakurai, The Journal of Physical Chemistry C 116 (2012) 26776–26783.
[33] J. Radnik, C. Mohr, P. Claus, Physical Chemistry Chemical Physics 5 (2003) 172–177.
[34] A.M. Venezia, L.F. Liotta, G. Pantaleo, V. La Parola, G. Deganello, A. Beck, Z. Koppány, K. Frey, D. Horváth, L. Guczi, Applied Catalysis A: General 251 (2003) 359–368.
[35] J.M. Coronado, A.J. Maira, J.C. Conesa, K.L. Yeung, V. Augugliaro, J. Soria, Langmuir 17 (2001) 5368–5374.
[36] T. Berger, O. Diwald, E. Knözinger, M. Sterrer, J.T. Yates Jr., Physical Chemistry Chemical Physics 8 (2006) 1822–1826.
[37] E.A. Konstantinova, A.I. Kokorin, S. Sakthivel, H. Kisch, K. Lips, CHIMIA International Journal for Chemistry 61 (2007) 810–814.
[38] M. Fittipaldi, M. Curri, R. Comparelli, M. Striccoli, A. Agostiano, N. Grassi, C. Sangregorio, D. Gatteschi, The Journal of Physical Chemistry C 113 (2009) 6221–6226.
[39] C. Langhammer, I. Zoric, B. Kasemo, B.M. Clemens, Nano Letters 7 (2007) 3122–3127.